THE JOURNAL OF PHYSICAL CHEMISTRY C

Article

pubs.acs.org/JPCC

Size-Dependent Chemical Reactivity of Silicon Nanocrystals with Water and Oxygen

Melanie L. Mastronardi,[†] Kenneth K. Chen,[†] Kristine Liao,[†] Gilberto Casillas,[‡] and Geoffrey A. Ozin*[,†]

[†]Department of Chemistry, University of Toronto, 80 St. George Street, Toronto, Ontario M5S 3H6, Canada

[‡]UOW Electron Microscopy Centre, University of Wollongong, Wollongong, New South Wales 2500, Australia

Supporting Information

ABSTRACT: A detailed investigation examines how the size of allylbenzene-capped silicon nanocrystals (ncSi:AB) affects their chemical reactivity with gaseous O_2, H_2O, and O_2/H_2O as probed by in situ luminescence spectroscopy. Specifically, changes in the photoluminescence (PL) of size-separated ncSi:AB are monitored through alterations of their PL absolute quantum yield (AQY) as well as the wavelength and intensity of their PL spectra over time. These experiments, conducted under both continuous and intermittent illumination, help elucidate the roles of O_2, H_2O, and mixtures of O_2/H_2O, with respect to oxidation of ncSi:AB as a function of their size, providing vital information for any perceived application in advanced materials and biomedical devices.

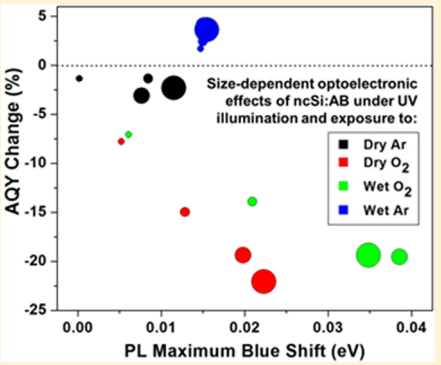

INTRODUCTION

Silicon nanocrystals (ncSi) were found to exhibit intense room-temperature photoluminescence in 1990,[1] and subsequent study has identified that they possess size-dependent optical and electronic properties,[2−5] similar to other semiconductor nanocrystals composed of heavy metal materials. In particular, quantum and spatial confinement effects result in a widening of the electronic band gap and a blue shift in photoluminescence (PL) as the ncSi particle size decreases.[2−6] Recent studies also report that ncSi show size-dependent PL absolute quantum yields (AQYs).[3,5,7,8] These size-dependent properties, as well as a wide PL range that spans the visible to near-infrared region,[5] have established ncSi as a promising candidate in optoelectronic and biological imaging applications.[9−13]

Currently, there are a variety of methods that exist for the synthesis of ncSi, including the annealing of SiO_x powders followed by etching with HF,[14] plasma synthesis,[15] and solution reduction of $SiCl_4$.[16] The colloidal stability of ncSi is easily achieved through a hydrosilylation reaction between surface Si−H groups and terminal alkenes.[17−19] Recently, it has been reported that thermal hydrosilylation can result in the oligomerization of ligands at the nanocrystal surface, an effect the authors report to be independent of ncSi size.[20] Regardless of whether the ncSi surface is capped by a monolayer or oligomers, it is well established that surface capping with organic ligands helps to prevent unwanted oxidation of the nanocrystal surface; however, over time even capped ncSi have been shown to oxidize under ambient conditions.[17,21−23] Exposure to air over time, resulting in surface oxidation, is known to quench the PL of ncSi as well as blue shift the emission wavelength.[8,21] The blue shifting of PL has traditionally been attributed to the shrinking of the nanocrystalline core due to the formation of an oxide layer,[6,24,25] in which the formation of dangling bonds and defect sites creates surface states in the band gap that effectively quench the PL.[26,27] Recently, an alternative defect site emission has been reported for the observed PL blue shifting of organically capped ncSi with surface oxidation.[28]

To date little is known regarding the role O_2 and H_2O play in oxidation processes for ligand-capped ncSi, but there are a variety of reports outlining different processes through which unfunctionalized or hydride-capped ncSi interact with H_2O and O_2.[26,29−31] Investigation of the oxidation of hydride-capped ncSi by electron spin resonance was reported to be consistent with the Cabrera−Mott theory of oxidation in ambient air.[26] The process is proposed to involve an induction period where the preferential adsorption of H_2O near surface silanol (Si−OH) groups aids the cleavage of an adjacent Si−Si bond, which transfers an electron to an adsorbed O_2 and attracts it to the cleaved bond. Reaction of the O_2 at this site then leads to the formation of two Si−O−Si groups. Studies of bulk-Si surfaces indicate that the duration of the induction period is inversely proportional to the humidity and density of Si−OH groups.[32,33]

Hydride-terminated ncSi (ncSi:H) have been shown to be efficient photosensitizers of singlet oxygen due to their long radiative lifetimes.[29,31] This process quenches the PL of ncSi as energy is transferred from optically excited excitons to O_2 molecules adsorbed on the ncSi surface and is most efficient at a PL wavelength of 760 nm (1.63 eV), which corresponds to the transition energy from the O_2 triplet state to the excited

Received: October 21, 2014
Revised: December 5, 2014
Published: December 7, 2014

   dx.doi.org/10.1021/jp510592j | J. Phys. Chem. C 2015, 119, 826−834

singlet state.[31] PL quenching has been shown to be a reversible effect provided that the ncSi:H have not been exposed to O_2 under prolonged illumination, which leads to an irreversible photooxidation process that degrades the PL permanently.[30] Singlet O_2 energy is not enough to break a Si−Si bond; therefore, thermal energy is also required for the formation of Si−O−Si, which has been reported to form more quickly at higher temperatures.[30]

While oxide formation at the ncSi surface tends to result in PL quenching, in some cases PL enhancement has also been observed; this is attributed to oxidation-induced passivation of dangling bonds.[6,34,35] It has been proposed that the apparent discrepancy between different studies may result from variations in initial surface passivation and oxidation conditions.[26] Overall the consensus is that interfacial defects and Si dangling bonds strongly influence the optoelectronic properties of ncSi,[26] which means that understanding the surface structure of ncSi and how it oxidizes is of the utmost importance for developing functional ncSi materials, particularly for colloidally stable ligand-capped ncSi of varying size.

In order to probe the effects of oxidation on different sizes of organic capped ncSi, we report the results of chemical reactivity studies performed on allylbenzene-capped ncSi (ncSi:AB) that have been size separated into relatively monodisperse fractions using size-selective precipitation.[3]

EXPERIMENTAL SECTION

Trichlorosilane ($HSiCl_3$, 99%) was purchased from Sigma-Aldrich, stored in a refrigerator, and used as received. Hydrofluoric acid (ACS reagent 48%, Sigma-Aldrich), ethanol (anhydrous, Commercial Alcohols), methanol (ACS reagent ≥99.8%, Sigma-Aldrich), toluene (anhydrous, Sigma-Aldrich), isopropanol (ACS, EMD), potassium hydroxide (technical grade, ACF), hexanes (ACS reagent, Caledon Laboratories), and phenyltriethoxysilane (98%, Aldrich) were used as received. Allylbenzene (98%, Aldrich) was filtered through activated neutral alumina (type WN-3, Sigma-Aldrich) and a 0.2 μm PTFE syringe filter before use to remove any peroxide impurities.[36] Argon compressed gas (ultrahigh purity, Praxair) and 49.9% oxygen balance argon compressed gas (certified standard, Praxair) were purged through deionized water or Drierite.

Size-separated allylbenzene-capped ncSi were synthesized using a previously reported method with some modifications.[3] This method involves the high-temperature thermal processing of sol−gel hydridosilicate ($HSiO_{1.5}$) glasses derived from trichlorosilane ($HSiCl_3$), followed by etching with HF to liberate the ncSi from the encapsulating SiO_2 matrix. The hydride-terminated ncSi were functionalized with allylbenzene groups using a thermally initiated hydrosilylation reaction in neat allylbenzene to produce a stable, concentrated colloidal dispersion. The ncSi that were too large to be stabilized with allylbenzene caps were removed from the reaction mixture by centrifugation. Vacuum distillation was used to isolate ncSi:AB from the excess unreacted allylbenzene, which was saved and recycled for future use. The ncSi:AB sample was then heated under a vacuum at 155 °C for 5.5 h to further remove excess alkenes trapped in the ligand shell.[37] The purified polydisperse ncSi:AB were redispersed in anhydrous toluene, resulting in a clear orange solution that displayed bright orange-red photoluminescence (PL) under photoexcitation (λ_{exc} = 365 nm). Size-selective precipitation was performed on the toluene dispersion of polydisperse ncSi:AB, using methanol as the antisolvent to isolate fractions of relatively monodisperse ncSi:AB. Following each addition of methanol, the cloudy solution was briefly sonicated then centrifuged for 10 min at 6461 rpm. The clear supernatant was decanted, and the solid was immediately redispersed in toluene. In order to ensure sample purity, each fraction was precipitated a second time. Immediately after the supernatant was decanted after the second precipitation the solid precipitate was transferred into a glovebox in order to minimize exposure of the precipitate to air and surface oxidation. In the glovebox, the solid precipitate for each fraction was dispersed in anhydrous toluene and stored until used.

Glass slide substrates were treated in a mixture of KOH and isopropanol (sonicated for 1 h and left overnight), then rinsed with distilled water and dried in an oven. Dried substrates were then coated with phenyltriethoxysilane and heated in an oven at around 120 °C for 3 days. The substrates were then rinsed with hexanes, dried, and transferred to a glovebox. An amount of 40 μL of a toluene dispersion of ncSi:AB was drop-coated onto each hydrophobic glass substrate and allowed to dry.

Scanning transmission electron microscopy (STEM) images were acquired in a probe-corrected JEOL ARM200F operated at 80 kV equipped with a cold field emission gun and a high-resolution pole piece. Middle angle annular dark-field (MAADF) images were acquired with 45 and 180 mrad inner and outer collection angles, respectively, while bright-field images used 11 mrad collection angles. Both images were recorded with a dwell time of 38 μs and a convergence semiangle of 25 mrad resulting in a probe current of 40 pA. Toluene dispersions were drop-cast onto graphene−Cu grids (Graphene Supermarket) to ensure an ultrathin support film of less than 2 nm. At least 500 particles were measured by hand to determine the average particle diameter and standard deviation values of the ncSi:AB from microscopy images. The photoluminescence of the ncSi:AB fractions was measured using the absolute quantum yield setup described below. The absolute quantum yield was determined using a previously reported integrating sphere method.[38] Samples were excited in an integrating sphere (Gigahertz Optik, custom-made) with light from a 365 nm LED (Thorlabs M365L2), and photoluminescence was collected by a 1 mm diameter optical fiber (Ocean Optics) and detected by an Ocean Optics Maya 2000 spectrometer. The continuous absolute quantum yield was measured by taking appropriate ratios of the excitation and emission peak areas of spectra recorded for the empty sphere and sample holder and the excitation focused directly onto the sample.[39] The accuracy of the system was verified against literature values for rhodamine 6G and MEH-PPV. Solution samples were measured in cuvettes that were filled and sealed in the glovebox. Film samples were sealed into a custom-made sample holder in the glovebox that was then inserted into the integrating sphere. During each measurement, the film samples were exposed to different atmospheres. The humidity of the atmospheres was monitored using a relative humidity probe (RH-USB, Omega Engineering, Inc.). Intermittant illumination was achieved by blocking the LED light from hitting the sample throughout the measurement. All AQY and PL film experiments were conducted in duplicate, and the extracted AQY and PL values were averaged wherever possible. PL spectra were smoothed and baseline corrected using Origin Pro 8 software. Fourier transform infrared (FTIR) spectroscopy was performed on a PerkinElmer Spectrum One FTIR spectrometer, and peak areas were determined using Spectrum software. For pristine

dx.doi.org/10.1021/jp510592j | J. Phys. Chem. C 2015, 119, 826−834

samples, films of ncSi:AB were drop-cast onto an IR transparent KBr substrate in the glovebox, covered with a second KBr substrate, and sealed with Teflon tape. For samples exposed to different atmospheres, films of ncSi:AB were drop-cast onto 6 mm by 1 mm KBr plates, loaded into the resealable continuous AQY sample holder in the glovebox, and exposed to the gas flow as above, under illumination in the integrating sphere or in the dark. The plates were then removed and run immediately under ambient conditions. X-ray photoelectron spectra (XPS) were obtained using a Thermo Scientific Theta Probe utilizing monochromatic Al Kα radiation. Spectra were calibrated to the C 1s emission arising from adventitious hydrocarbons (284.8 eV). The high-resolution Si 2p region of the XPS was fit for the dominant Si species (Si^0, Si^{1+}, Si^{2+}, Si^{3+}, and Si^{4+}). Atomic % analysis was determined by converting background-corrected areas of the C 1s, O 1s, and Si $2p^0$ peaks to relative atomic % with sensitivity factors and a correcting energy compensation factor using Advantage software.

RESULTS AND DISCUSSION

The polydisperse ensemble and select size-separated ncSi:AB samples were characterized by scanning transmission electron microscopy (STEM). Particle size analysis confirms the expected decreasing particle size with increasing size-selective precipitation step (Supporting Information (SI) Figure 1). The average diameter values were measured as 2.79 ± 1.7 nm for the ensemble, 2.22 ± 0.5 nm for fraction 11, 2.14 ± 0.4 nm for fraction 13, 2.01 ± 0.4 nm for fraction 16, and 1.81 ± 0.4 nm for fraction 18. All fractions contain some degree of crystallinity, with crystal lattice lines appearing in the images of all samples examined. However, lattice fringes are not observed for all particles, which may be due to random orientation of the particles and beam damage that causes the particles to amorphize before an image can be acquired. It is not possible to say if all particles were crystalline to begin with, but there is certainly crystallinity observed for even the smallest particles that were imaged (SI Figure 2).

Select pristine samples of size-separated ncSi:AB were analyzed using FTIR spectroscopy. The FTIR spectrum shown for fraction 11 (Figure 1A, inset) shows the characteristic stretching modes associated with ncSi:AB, consistent with previous work.[3] To compare the surface species present for fractions of different size, ratios of select areas associated with Si−H, C−H, and Si−O−Si/Si−OR stretching modes are plotted in Figure 1A. The ratio of the C−H to Si−H areas increases slightly with decreasing size, indicating that there is a higher proportion of allylbenzene ligands to Si−H species at the surface of smaller ncSi:AB. This can be explained by the increasing surface curvature of particles with decreasing size. Complete surface coverage of ncSi with any alkyl ligand is not possible due to the disparity between the diameter of an alkyl chain carbon (4.2 Å) and the spacing between silicon atoms on the Si surface (3.85 Å for 111).[40] Ligand cone models have been reported and used to estimate the surface coverage of ligands on nanoparticle surfaces.[41] For allylbenzene, which has a higher ligand cone angle compared to a linear alkyl group, a higher surface curvature will allow more room for ligands to spread out from the nanocrystal surface, allowing more Si−H species to be converted to Si−AB with decreasing particle size. The presence of adventitious surface oxidation has been reported in previous syntheses of organic capped ncSi,[11,42] and despite our best efforts to minimize exposure to air and oxide species during the synthesis and separation, FTIR spectra

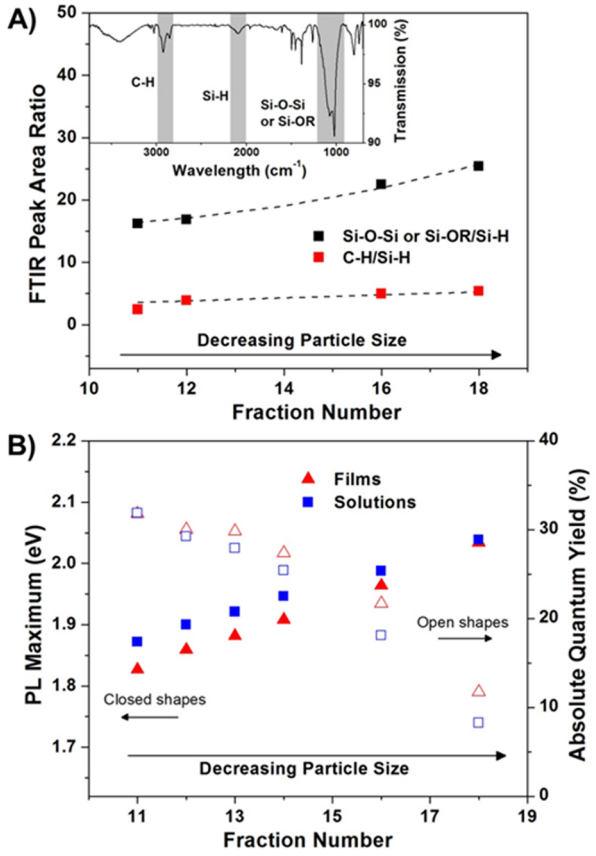

Figure 1. (A) Ratios of FTIR peak areas plotted for select size-separated ncSi:AB fractions. Inset: denotes peak area regions examined on the FTIR spectrum of fraction 11. (B) Photoluminescence (PL) maximum and PL absolute quantum yield plotted versus fraction number for both film and solution samples.

of the ncSi:AB fractions indicate the presence of adventitious surface oxidation. The ratio of the peak associated with Si−O−Si or Si−OR to Si−H increases with decreasing size, indicating that a greater proportion of oxide species exist at the ncSi:AB surface of smaller particles. This size-dependent adventitious surface oxidation trend is also observed in comparing the relative atomic % of core Si, O, and C species determined by XPS for particles of varying size (SI Figure 3A, 4). The Si−H species that remain at the ncSi:AB surface likely react with oxygen during the brief air exposure in the size-separation process when transferring the precipitate to the glovebox or with methanol, which was used as the antisolvent in the size-separation step.[43] The size dependence of the adventitious surface oxidation may be explained by the increasing spacing between the ligand tails that make it easier for oxide species to reach the surface with increasing curvature;[44] however, due to the fact that smaller sized particles were exposed to methanol for longer time periods during the size-separation process, it is likely that extended exposure to methanol is responsible for the observed oxidation trend. Despite the presence of oxide surface species, there is still a significant peak associated with Si−H for all fractions, indicating the presence of sites with which oxygen species in the O_2- and H_2O-rich environments studied in this work can interact.

The PL spectra and PL AQY were measured for select pristine fractions of ncSi:AB both dispersed in toluene and drop-coated onto treated hydrophobic glass slide substrates. The PL maximum blue shifts with decreasing particle size for

dx.doi.org/10.1021/jp510592j | J. Phys. Chem. C 2015, 119, 826−834

both film and solution samples (Figure 1B). While a PL blue shift is generally considered to be consistent with the effects of quantum confinement,[7,27] we note a red shift of the PL maximum of the ncSi:AB fractions compared to theoretical relationships for the same ncSi size (SI Figure 5).[6,45] This discrepancy is attributed to surface effects. Computational work on ncSi particles shows that the band gap energy is dependent on surface capping; in particular, the band gap decreases (or red shifts) slightly for ncSi capped with alkyl groups compared to hydride caps.[46] For the ncSi:AB examined here with the presence of adventitious oxidation, it is also possible that the emission energy is altered by the presence of Si═O species that are reported to create new midgap electronic states in the electronic structure of ncSi below 3 nm.[45] Since the synthesized ncSi:AB range is from 1.5 to 3 nm, in the presence of Si═O, recombination is proposed to occur between a free hole and a trapped electron whose energy is size independent. The PL energy increases as particle size decreases, although not as fast as predicted by quantum confinement, which is consistent with the PL trends observed for size-separated ncSi:AB (SI Figure 5). It has also recently been reported that the PL of ncSi can be tuned independent of size with different types of surface ligands, and PL observed ranging from orange to blue is attributed to short-lived surface excited states or a combination of excited states and band gap emission.[28] Dasog et al. showed PL excited state lifetimes measured on the nanosecond range for dodecyl-capped ncSi hydrosilylated in air to give partial surface oxidation, which are attributed to an unidentified surface state.[28] Previously reported lifetimes between 20 and 60 μs for ncSi:AB synthesized and separated in the same manner as reported here[3] suggest that despite the presence of adventitious surface oxidation the size-dependent PL trend is the result of band gap emission and a combination of surface and quantum confinement effects. A slight red shift in PL peak emission for film versus solution samples is attributed to greater particle interactions in the solid-state film samples, resulting in interparticle coupling or efficient energy transfer from the smaller particles to the larger particles.[47,48]

The AQY shows a decreasing trend with decreasing particle size for both film and solution samples (Figure 1B), which is consistent with previous reports of similarly sized ncSi.[3,8] In previous work, the AQY decrease is attributed to a decrease in ncSi core crystallinity with decreasing particle size, as well as an increase in competing nonradiative relaxation surface trap and defect pathways that become more prevalent with decreasing ncSi size.[3] The microscopy and FTIR results presented here tend to favor the latter explanation since some crystallinity is observed for even the smallest particles imaged, and the ratio of oxide species, likely to contribute to surface traps and defect sites, is shown to increase with decreasing particle size.

In order to probe the effect different oxygen species have on the optical properties of ncSi:AB, the AQY was measured continuously while film samples of select fractions were exposed to different atmospheres. Initially each sample was prepared and sealed under nitrogen; the samples were then exposed to one of the following atmospheres: dry argon, wet argon, dry 50% oxygen in argon (referred to as dry O_2), and wet 50% oxygen in argon (referred to as wet O_2). PL spectra were measured initially and after exposure to each atmosphere for 300 s. To help elucidate the extent of nonchemical quenching observed select films were subsequently purged with dry Ar following exposure to O_2 and H_2O containing atmospheres. In addition to the continuous AQY measurements outlined above, film samples were run under all atmospheres with intermittent illumination to study the effect of light on the reactivity of H_2O and/or O_2 species at the ncSi:AB surface.

AQY curves and relative humidity curves representative of wet and dry conditions under continuous illumination are shown for fraction 16 in Figure 2A, with the corresponding PL

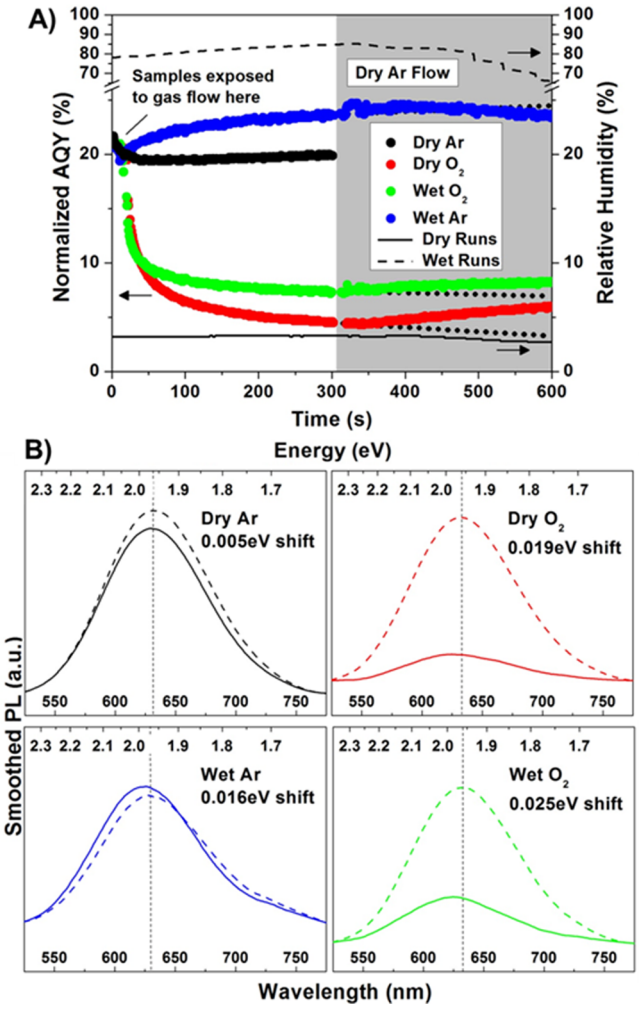

Figure 2. (A) Photoluminescence (PL) absolute quantum yield (AQY) curves for fraction 16 measured under different atmospheres, showing representative relative humidity curves for dry and wet atmospheres. The AQY curves have been normalized to the average initial AQY value. After 300 s the atmospheres containing H_2O and/or O_2 were purged for 300 s with dry Ar flow through the system. The dotted lines shown following the switch to dry Ar are guides to help visualize the changes in AQY. (B) PL spectra for fraction 16 measured before (dashed line) and after exposure (solid line) to each atmosphere for 300 s. PL spectra have been smoothed for clarity. PL blue shift from the initial value for each atmosphere is denoted in eV.

spectra shown in Figure 2B. In the analysis of these results, it is useful to assume a baseline with the results of inert dry Ar exposure at 300 s where the signals have stabilized in order to measure and understand the effects of H_2O and O_2. Despite efforts to purge and eliminate air from the testing apparatus, it is likely that some residual ambient air remained; this is demonstrated by a slight decrease in AQY (from 22 to 20%) and slight blue shift in PL maximum (0.005 eV) observed for

dx.doi.org/10.1021/jp510592j | J. Phys. Chem. C 2015, 119, 826−834

the P16 dry Ar sample. Recent work suggests that exposure to UV light under inert conditions results in a decrease in AQY due to nonoxidative photobleaching,[49] which may also be contributing to the decrease in AQY we observe. However, the work presented here was performed on a much shorter time scale and shows a blue shift in PL indicating that oxidation from residual air is likely the dominant contributing effect.

Upon exposure to atmospheres containing O_2 (both wet and dry) a significant decrease in AQY was observed. At 300 s, AQY values were 7% and 4.5% for samples exposed to wet O_2 and dry O_2, respectively. Additionally, PL blue shifts for both dry (0.019 eV) and wet O_2 (0.025 eV) were observed. Since blue shifting of ncSi emission energy has been attributed to oxidation for ncSi exposed to air overtime, it can be inferred that some form of irreversible oxidation is occurring for samples in all atmospheres. This oxidation would also result in some PL quenching (decrease in AQY) due to the emergence of intermediate states caused by the formation of dangling bonds and defect sites.[26,27] The large AQY decrease and PL blue shift observed for both samples exposed to O_2 indicate that surface oxidation is responsible for a large extent of the optoelectronic changes.

Purging with dry Ar beginning at 300 s results in an increase of the AQY of dry O_2 treated ncSi:AB from 4.5 to 6% and an increase from 7 to 8% for wet O_2 treated samples by 600 s. On the basis of this increase in AQY, it is proposed that the AQY decrease observed at 300 s is due to a combination of defect states formed from irreversible surface oxidation as well as photosensitization, which would give some reversible PL quenching. Photosensitization in this case describes the process where the formation of photogenerated singlet oxygen molecules results in the photodegradation of ncSi.[30] Molecular oxygen adsorbed to ncSi surfaces acts as a competing mechanism through which photogenerated excitons within the ncSi may transfer its energy, leading to the generation of singlet oxygen. The reactive singlet oxygen may then react with the ncSi surface, leading to irreversible photooxidation. It is likely that the dry Ar purge after 300 s removed some of the adsorbed oxygen to reduce its depressing effect on the AQY.

The contribution of H_2O on irreversible surface oxidation and photosensitization is difficult to quantify, but by comparing the results of wet and dry O_2 exposure in Figure 2, a few trends are observed. The larger initial AQY decrease and lower AQY increase with dry Ar purging for wet O_2 compared to dry O_2 (Figure 2A) suggests that a greater extent of irreversible surface oxidation versus photosensitization is contributing to the AQY changes in the wet O_2 atmosphere. Additionally, a larger blue shift is observed for wet O_2 (0.025 eV) compared to dry O_2 (0.019 eV) (Figure 2B). These results are consistent with reports where H_2O passivates dangling bonds generated by oxidation by forming Si−OH groups,[26] and higher humidity with higher density of Si−OH groups helps shorten the induction period for surface oxidation of ncSi.[32,33]

In Figure 2, ncSi:AB exposed to wet Ar shows an increase in AQY up to 4% above the dry Ar baseline, with a PL blue shift (0.016 eV) that is 3 times greater than that of ncSi:AB exposed dry Ar after 300 s. The larger blue shift compared to dry Ar is likely the result of residual air in the system, as previously described, that in the presence of H_2O would be much more likely to oxidize the surface. It has been proposed that physisorbed H_2O may be responsible for air-induced PL degradation of ncSi;[49] however, in the presence of a small amount of residual air and excess H_2O we see an overall enhancement of the PL, despite the observed PL blue shift attributed to oxidation from residual air. The observed increase in AQY is attributed to the passivation of defects states and dangling bonds present on the ncSi:AB surface by the excess H_2O in the atmosphere.[26] With dry Ar purging after 300 s, the AQY continues to increase slightly and then begins to decline after about 450 s. Assuming the interaction between ncSi:AB and pure H_2O to passivate defects takes place as both a chemical reaction and physical adsorption, removing some of the excess H_2O with dry Ar purging could result in reducing the passivation effect, thereby decreasing the AQY.

Since a source of photogenerated excitons is a key to photosensitization of O_2 and subsequent photooxidation, an experiment with intermittent illumination, rather than continuous illumination, and AQY measurement was conducted as shown in Figure 3A. The results show that when intermittent illumination is used the overall effect of each atmosphere on the AQY is not as severe as with continuous illumination, indicating the strong role of light in the interaction between H_2O and O_2 with the ncSi:AB surface. At 300 s of exposure, despite the presence of some residual air, the AQY for ncSi:AB exposed to dry Ar remains stable at approximately 20.5%. Intermittent illumination results in minimizing the AQY decrease for ncSi:AB in dry O_2, reaching only about 8.5% instead of 4.5% under continuous illumination after 300 s. In wet O_2, the

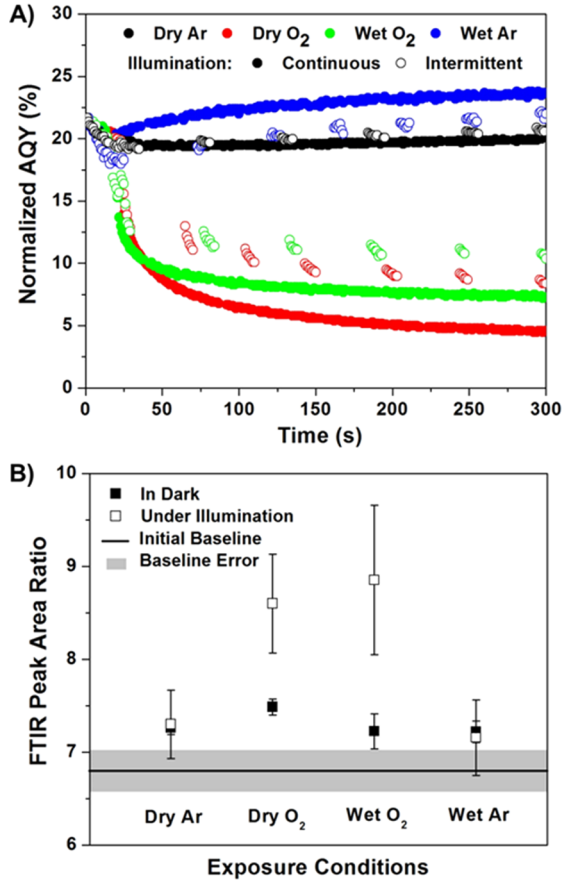

Figure 3. (A) Absolute quantum yield (AQY) curves for fraction 16 measured under different atmospheres with continuous and intermittent illumination. (B) Ratio of the Si−O−Si/Si−OR to Si−H peak areas for fraction 10 after exposure to different conditions under continuous illumination and in the dark for 300 s, compared to the initial baseline ratio of pristine ncSi:AB.

dx.doi.org/10.1021/jp510592j | J. Phys. Chem. C 2015, 119, 826−834

ncSi:AB AQY decrease is minimized as well but to a slightly lower extent, reaching only about 10% instead of 7% under continuous illumination. The lower decreases observed for O_2-exposed samples are consistent with previously reported work of polydisperse ncSi exposed to air, with and without UV illumination.[49] The ncSi:AB exposed to wet Ar increases to about 22%, which is slightly lower than the value of 24% achieved under continuous illumination, indicating that the passivation of surface defects is promoted with additional energy.

To clarify the role light plays on irreversible surface oxidation and ultimately the AQY and PL maximum, FTIR measurements were taken for film samples of fraction 10 drop-coated on KBr windows that were subject to the four atmospheres under continuous illumination and in the dark. The area ratios of peaks assigned to the Si−H (2100 cm^{-1}) and Si−O−Si/Si−OR (1090 cm^{-1}) stretches are plotted in Figure 3B, along with the initial baseline ratio measured before exposure to the atmospheres. While there are only small differences in the ratio for the samples exposed to wet and dry Ar, both dry and wet O_2-exposed samples show a significantly higher ratio under continuous illumination, which is evidence of the extent photooxidation contributes to the formation of Si−O−Si and Si−OR species and the optoelectronic changes observed. FTIR spectra, as well as XPS data (SI Figure 3B, 4), also suggest that allylbenzene ligands are retained on the ncSi surface upon oxidation. Unfortunately, the extent of Si−OH on the ncSi:AB surface cannot be probed using FTIR under wet and dry conditions as the Si−OH peak overlaps with the peak associated with adsorbed H_2O in the region between 3200 and 3600 cm^{-1}.

Continuous AQY curves and PL spectra (similar to those described above for fraction 16) were measured for film samples of four different sized fractions (11, 13, 16, and 18). The difference in the PL AQY value (AQY final − AQY initial) for each fraction exposed to each atmosphere is plotted in Figure 4A. Similar results as previously outlined for fraction 16 are observed for all sizes examined, where the decrease in AQY is greatest for samples exposed to dry O_2, followed by wet O_2, then dry Ar, and samples exposed to wet Ar show an increase in AQY. Size-dependent trends can also be extracted from these results, where the AQY decrease increases in magnitude as the particle size increases for films exposed to dry Ar, dry O_2, and wet O_2. Work examining photosensitization of porous silicon suggests that larger particles show the greatest PL degradation due to their larger surface region, which would increase the probability of O_2 interacting at the surface.[30] Despite the presence of ligands at the ncSi:AB surface, this effect may also occur here, such that more PL quenching is possible for the largest particles. This trend may also be explained by the fact that quenching by photosensitization is most efficient when the PL energy occurs at 1.63 eV (760 nm).[31] The PL spectra of all fractions have some intensity at this energy, but as the particle size decreases the PL maximum blue shifts away from this value so the smaller particles have less overlap with the preferred photosensitization wavelength compared to the largest particles.

In the case where the films are exposed to wet Ar, the AQY increase increases in magnitude with increasing size. This trend may also be explained by larger particles having larger surfaces, which likely results in a higher number of surface defects with which H_2O is able to interact and passivate.

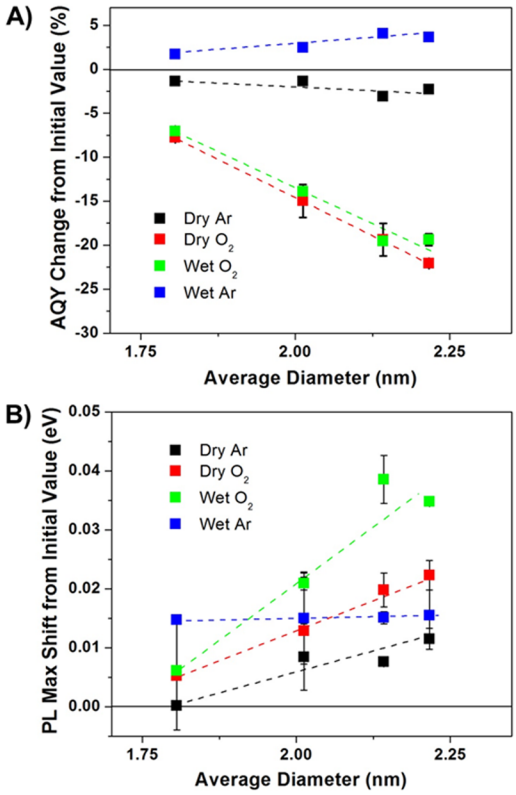

Figure 4. Size-dependence of photoluminescence (PL) maximum shift and PL absolute quantum yield (AQY) change. (A) The value by which the PL AQY changes after exposure to various atmospheres compared to its initial value is plotted for different sized fractions. (B) The value by which the PL maximum shifts after exposure to various atmospheres compared to its initial PL maximum is plotted for different sized fractions. In both (A) and (B), dashed lines are shown to visually illustrate the size-dependent trends, and where error bars are not visible, the associated error value falls within the range of the symbol size.

The PL blue shift (final PL maximum − initial PL maximum) in eV for fractions exposed to all atmospheres (Figure 4B) appears to show a size-dependent trend in which a larger PL blue shift is observed for larger particles for all conditions except wet Ar. Assuming the blue shifting of ncSi emission energy is the result of the shrinking of the nanocrystalline core with oxidation,[24] it is possible that the larger particles have the ability to blue shift more than smaller particles, since as illustrated in the SI Figure 5 the PL blue shift (or band gap energy increase) of the ncSi:AB for both film and solution samples decreases in magnitude with decreasing size. As noted previously, this variation from the expected theoretical relationship between band gap and particle size is attributed to the effect of surface species, and in keeping with this and the size-dependent PL blue shift trends observed, it has previously been reported that particles that have less initial surface oxidation show greater PL blue shifting upon further oxidation.[50] This fits well with the FTIR (Figure 1A) and XPS (SI Figure 3A) measurements of pristine ncSi:AB presented here showing that the smaller particles initially possess a larger extent of surface oxidation. XPS measurements of size-separated ncSi:AB exposed to air for an extended period of time show a greater relative atomic % of oxygen for larger particles (SI Figure 3B) and almost no atomic % of core silicon for the smallest fraction examined, indicating that the limiting

dx.doi.org/10.1021/jp510592j | J. Phys. Chem. C 2015, 119, 826−834

Scheme 1. Summary of Some Proposed Interactions That May Be Occurring at the ncSi:AB Surface under Each Atmosphere and UV Illumination

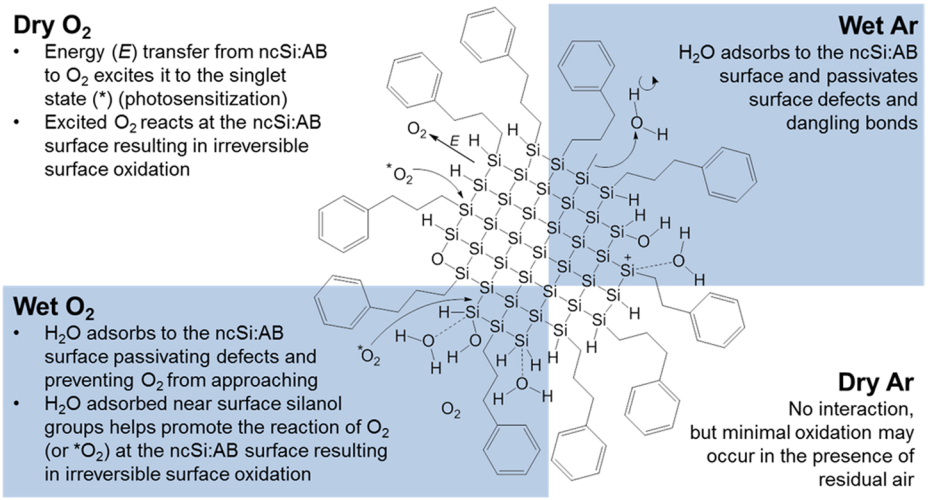

factor for the overall extent of oxidation possible is the size of the ncSi core. The PL shift magnitude and slope of each trend generally follows the order where wet O_2 > dry O_2 > dry Ar, which is consistent with the results previously explained for fraction 16, where the presence of H_2O with O_2 helps promote the irreversible oxidation of the ncSi:AB surface. Under exposure to wet Ar, the interaction of ncSi:AB with H_2O has a significant effect on the PL maximum, resulting in a shift of about 0.015 eV for all sizes. While PL shifting is likely to occur from surface oxidation from residual air in the system, the lack of size dependence observed for wet Ar on the PL maximum of ncSi:AB indicates that there may be size-independent surface effects that are responsible for the PL blue shift observed. More extensive study, however, is required to confirm and identify the effects responsible for the observations in wet Ar.

In this study, we have shown that by quantitatively monitoring the effects O_2, H_2O, and O_2/H_2O environments have on the PL wavelength, intensity, and AQY of ncSi:AB one can obtain valuable insight into the effect of the size of the silicon core on chemical reactivity. While these results do not allow for the definitive assignment of the reactions occurring at the ncSi:AB surface with O_2, H_2O, and O_2/H_2O, some of the dominant interactions proposed to be occurring under each atmosphere are illustrated in Scheme 1. The interactions denoted in this scheme are not meant to be comprehensive but have been included to help illustrate the results reported herein. With the collected results of this investigation it behooves one to think about the molecules and materials effects that most likely contribute to the trends observed for the size-dependent reactivity of ncSi:AB with O_2, H_2O, and O_2/H_2O.

It is clear from the results presented in this paper that both O_2 and H_2O and mixtures thereof can oxidize the silicon core of ncSi:AB. Within the range of sizes examined, there are a variety of contributing factors to consider. While one can imagine that the higher the curvature of a smaller silicon nanocrystal core the easier the diffusion of O_2 and H_2O through the allylbenzene corona to facilitate oxidation of the core, the increased reactivity observed with increasing size suggests that this effect does not play a significant role here. In keeping with the trends observed, the smaller the silicon nanocrystal core with its larger electronic band gap and higher ionization potential, the harder it would be to oxidize with O_2, H_2O, and O_2/H_2O. Additional factors required to understand the size-dependent oxidation trends include the surface area of the silicon core, which relates to the number of surface defects present per ncSi:AB, and the number of H_2O or O_2 species that can interact with the silicon core, related to the relative amounts of excess species introduced in the atmosphere versus the small amount of residual air likely present in the system. The initial presence of oxide species on the ncSi:AB surface also plays an important role, as well as the particle dimension, which limits the kinetics and extent of oxidation possible of the silicon core. Within the framework of this simple model, the surface area, initial surface oxidation, and electronic factors clearly favor increased chemical reactivity toward H_2O or O_2 as the size of ncSi:AB increases from 1.8 to 2.2 nm.

■ CONCLUSIONS

In this chemical reactivity study, the effects of O_2, H_2O, and a combination of both on the PL and AQY of relatively monodisperse ncSi:AB have been investigated for fractions of varying size. We have shown that O_2 alone is capable of quenching and blue shifting PL and that PL quenching likely occurs from a combination of reversible photosensitization and irreversible surface oxidation. In the presence of H_2O, the PL quenching that occurs from O_2 is minimized, and PL blue shifting is increased, likely due to the passivation of surface defects and dangling bonds by H_2O to create Si−OH species that help promote further irreversible surface oxidation by O_2 in the presence of H_2O. Exposure to H_2O alone results in an increase in the AQY. In all environments, the AQY changes observed increase with increasing particle size, and with the exception of exposure to wet Ar, the PL shifts observed increase with increasing size. Furthermore, in this work we have also shown that the chemical reactivity of the ncSi:AB surface with H_2O and/or O_2 is increased under continuous illumination with UV light. The collected results of this study provide vital information for any perceived application in advanced materials and biomedical devices.

dx.doi.org/10.1021/jp510592j | J. Phys. Chem. C 2015, 119, 826−834

■ ASSOCIATED CONTENT

Supporting Information

Scanning transmission electron microscopy images, XPS data, and a comparison of PL emission to size. This material is available free of charge via the Internet at http://pubs.acs.org.

■ AUTHOR INFORMATION

Corresponding Author

*E-mail: gozin@chem.utoronto.ca.

Notes

The authors declare no competing financial interest.

■ ACKNOWLEDGMENTS

The strong and sustained financial support of this research by the Natural Science and Engineering Research Council of Canada (NSERC) is deeply appreciated. A Premier Research Award in support of this research from the Ministry of Research Innovation (MRI) Ontario is also gratefully acknowledged. GAO is Government of Canada Tier 1 Canada Research Chair in Materials Chemistry. MLM is a Vanier Canada Graduate Scholar. This research used equipment funded by the Australian Research Council (ARC) - Linkage, Infrastructure, Equipment and Facilities (LIEF) grant (LE120100104) located at the UOW Electron Microscopy Centre. Dr. Peter Brodersen and Surface Interface Ontario are thanked for XPS measurements.

■ REFERENCES

(1) Canham, L. T. Silicon Quantum Wire Array Fabrication by Electrochemical and Chemical Dissolution of Wafers. *Appl. Phys. Lett.* **1990**, *57*, 1046−1048.

(2) Wilson, W. L.; Szajowski, P. F.; Brus, L. E. Quantum Confinement in Size-Selected, Surface-Oxidized Silicon Nanocrystals. *Science* **1993**, *262*, 1242−1244.

(3) Mastronardi, M. L.; Maier-Flaig, F.; Faulkner, D.; Henderson, E. J.; Kübel, C.; Lemmer, U.; Ozin, G. A. Size-Dependent Absolute Quantum Yields for Size-Separated Colloidally-Stable Silicon Nanocrystals. *Nano Lett.* **2012**, *12*, 337−342.

(4) Mastronardi, M. L.; Hennrich, F.; Henderson, E. J.; Maier-Flaig, F.; Blum, C.; Reichenbach, J.; Lemmer, U.; Kübel, C.; Wang, D.; Kappes, M. M.; et al. Preparation of Monodisperse Silicon Nanocrystals Using Density Gradient Ultracentrifugation. *J. Am. Chem. Soc.* **2011**, *133*, 11928−11931.

(5) Hessel, C. M.; Reid, D.; Panthani, M. G.; Rasch, M. R.; Goodfellow, B. W.; Wei, J.; Fujii, H.; Akhavan, V.; Korgel, B. A. Synthesis of Ligand-Stabilized Silicon Nanocrystals with Size-Dependent Photoluminescence Spanning Visible to near-Infrared Wavelengths. *Chem. Mater.* **2012**, *24*, 393−401.

(6) Ledoux, G.; Guillois, O.; Porterat, D.; Reynaud, C.; Huisken, F.; Kohn, B.; Paillard, V. Photoluminescence Properties of Silicon Nanocrystals as a Function of Their Size. *Phys. Rev. B: Condens. Matter Mater. Phys.* **2000**, *62*, 15942−15951.

(7) Miller, J. B.; Van Sickle, A. R.; Anthony, R. J.; Kroll, D. M.; Kortshagen, U. R.; Hobbie, E. K. Ensemble Brightening and Enhanced Quantum Yield in Size-Purified Silicon Nanocrystals. *ACS Nano* **2012**, *6*, 7389−7396.

(8) Rinck, J.; Schray, D.; Kübel, C.; Powell, A. K.; Ozin, G. A. Size-Dependent Oxidation of Monodisperse Silicon Nanocrystals with Allylphenylsulfide Surfaces. *Small* **2014**, DOI: 10.1002/smll.201401965.

(9) Wu, C.; Bull, B.; Szymanski, C.; Christensen, K.; McNeill, J. Multicolor Conjugated Polymer Dots for Biological Fluorescence Imaging. *ACS Nano* **2008**, *2*, 2415−2423.

(10) Henderson, E. J.; Shuhendler, A. J.; Prasad, P.; Baumann, V.; Maier-Flaig, F.; Faulkner, D. O.; Lemmer, U.; Wu, X. Y.; Ozin, G. A. Colloidally Stable Silicon Nanocrystals with near-Infrared Photoluminescence for Biological Fluorescence Imaging. *Small* **2011**, *7*, 2507−2516.

(11) Mastronardi, M. L.; Henderson, E. J.; Puzzo, D. P.; Chang, Y.; Wang, Z. B.; Helander, M. G.; Jeong, J.; Kherani, N. P.; Lu, Z.; Ozin, G. A. Silicon Nanocrystal Oleds: Effect of Organic Capping Group on Performance. *Small* **2012**, *8*, 3647−3654.

(12) Cheng, K. Y.; Anthony, R.; Kortshagen, U. R.; Holmes, R. J. High-Efficiency Silicon Nanocrystal Light-Emitting Devices. *Nano Lett.* **2011**, *11*, 1952−1956.

(13) Cheng, K. Y.; Anthony, R.; Kortshagen, U. R.; Holmes, R. J. Hybrid Silicon Nanocrystal-Organic Light-Emitting Devices for Infrared Electroluminescence. *Nano Lett.* **2010**, *10*, 1154−1157.

(14) Liu, S. M.; Yang, Y.; Sato, S.; Kimura, K. Enhanced Photoluminescence from Si Nano-Organosols by Functionalization with Alkenes and Their Size Evolution. *Chem. Mater.* **2006**, *18*, 637−642.

(15) Pi, X. D.; Liptak, R. W.; Deneen Nowak, J.; Wells, N. P.; Carter, C. B.; Campbell, S. A.; Kortshagen, U. Air-Stable Full-Visible-Spectrum Emission from Silicon Nanocrystals Synthesized by an All-Gas-Phase Plasma Approach. *Nanotechnology* **2008**, *19*, 245603.

(16) Zou, J.; Sanelle, P.; Pettigrew, K. A.; Kauzlarich, S. M. Size and Spectroscopy of Silicon Nanoparticles Prepared Via Reduction of Sicl4. *J. Cluster Sci.* **2006**, *17*, 565−578.

(17) Buriak, J. M. Illuminating Silicon Surface Hydrosilylation: An Unexpected Plurality of Mechanisms. *Chem. Mater.* **2014**, *26*, 763−772.

(18) Kelly, J. A.; Shukaliak, A. M.; Fleischauer, M. D.; Veinot, J. G. C. Size-Dependent Reactivity in Hydrosilylation of Silicon Nanocrystals. *J. Am. Chem. Soc.* **2011**, *133*, 19015−19016.

(19) Kelly, J. A.; Veinot, J. G. C. An Investigation Into Near-Uv Hydrosilylation of Freestanding Silicon Nanocrystals. *ACS Nano* **2010**, *4*, 4645−4656.

(20) Yang, Z.; Iqbal, M.; Dobbie, A. R.; Veinot, J. G. C. Surface-Induced Alkene Oligomerization: Does Thermal Hydrosilylation Really Lead to Monolayer Protected Silicon Nanocrystals? *J. Am. Chem. Soc.* **2013**, *135*, 17595−17601.

(21) Jurbergs, D.; Rogojina, E.; Mangolini, L.; Kortshagen, U. Silicon Nanocrystals with Ensemble Quantum Yields Exceeding 60%. *Appl. Phys. Lett.* **2006**, *88*, 233116.

(22) Jariwala, B. N.; Dewey, O. S.; Stradins, P.; Ciobanu, C. V.; Agarwal, S. In Situ Gas-Phase Hydrosilylation of Plasma-Synthesized Silicon Nanocrystals. *ACS Appl. Mater. Interfaces* **2011**, *3*, 3033−3041.

(23) Pi, X.; Wang, R.; Yang, D. Density Functional Theory Study on the Oxidation of Hydrosilylated Silicon Nanocrystals. *J. Mater. Sci. Technol.* **2014**, *30*, 639−643.

(24) Anthony, R.; Kortshagen, U. Photoluminescence Quantum Yields of Amorphous and Crystalline Silicon Nanoparticles. *Phys. Rev. B* **2009**, *80*, 115407.

(25) Gupta, A.; Swihart, M. T.; Wiggers, H. Luminescent Colloidal Dispersion of Silicon Quantum Dots from Microwave Plasma Synthesis: Exploring the Photoluminescence Behavior Across the Visible Spectrum. *Adv. Funct. Mater.* **2009**, *19*, 696−703.

(26) Pereira, R. N.; Rowe, D. J.; Anthony, R. J.; Kortshagen, U. Oxidation of Freestanding Silicon Nanocrystals Probed with Electron Spin Resonance of Interfacial Dangling Bonds. *Phys. Rev. B: Condens. Matter Mater. Phys.* **2011**, *83*, 155327.

(27) Delley, B.; Steigmeier, E. F. Quantum Confinement in Si Nanocrystals. *Phys. Rev. B* **1993**, *47*, 1397−1400.

(28) Dasog, M.; De los Reyes, G. B.; Titova, L. V.; Hegmann, F. A.; Veinot, J. G. C. Size Vs Surface: Tuning the Photoluminescence of Freestanding Silicon Nanocrystals Across the Visible Spectrum Via Surface Groups. *ACS Nano* **2014**, *8*, 9636−9648.

(29) Konstantinova, E. A.; Demin, V. A.; Vorontzov, A. S.; Ryabchikov, Y. V.; Belogorokhov, I. A.; Osminkina, L. A.; Forsh, P. A.; Kashkarov, P. K.; Timoshenko, V. Y. Electron-Paramagnetic Resonance and Photoluminescence Study of Si Nanocrystals-Photosensitizers of Singlet Oxygen Molecules. *J. Non-Cryst. Solids* **2006**, *352*, 1156−1159.

(30) Kovalev, D.; Gross, E.; Diener, J.; Timoshenko, V. Y.; Fujii, M. Photodegradation of Porous Silicon Induced by Photogenerated Singlet Oxygen Molecules. *Appl. Phys. Lett.* **2004**, *85*, 3590−3592.
(31) Kovalev, D.; Gross, E.; Künzner, N.; Koch, F.; Yu, T. V.; Fujii, M. Resonant Electronic Energy Transfer from Excitons Confined in Silicon Nanocrystals to Oxygen Molecules. *Phys. Rev. Lett.* **2002**, *89*, 1374011−1374014.
(32) Miura, T. A.; Niwano, M.; Shoji, D.; Miyamoto, N. Kinetics of Oxidation on Hydrogen-Terminated Si(100) and (111) Surfaces Stored in Air. *J. Appl. Phys.* **1996**, *79*, 4373−4380.
(33) Niwano, M.; Kageyama, J. i.; Kurita, K.; Kinashi, K.; Takahashi, I.; Miyamoto, N. Infrared Spectroscopy Study of Initial Stages of Oxidation of Hydrogen-Terminated Si Surfaces Stored in Air. *J. Appl. Phys.* **1994**, *76*, 2157−2163.
(34) Švrček, V.; Sasaki, T.; Shimizu, Y.; Koshizaki, N. Blue Luminescent Silicon Nanocrystals Prepared by Ns Pulsed Laser Ablation in Water. *Appl. Phys. Lett.* **2006**, *89*, 213113.
(35) Li, S.; Silvers, S. J.; El-Shall, M. S. Surface Oxidation and Luminescence Properties of Weblike Agglomeration of Silicon Nanocrystals Produced by a Laser Vaporization−Controlled Condensation Technique. *J. Phys. Chem. B* **1997**, *101*, 1794−1802.
(36) Stewart, M. P.; Buriak, J. M. Exciton-Mediated Hydrosilylation on Photoluminescent Nanocrystalline Silicon. *J. Am. Chem. Soc.* **2001**, *123*, 7821−7830.
(37) Panthani, M. G.; Hessel, C. M.; Reid, D.; Casillas, G.; José-Yacamán, M.; Korgel, B. A. Graphene-Supported High-Resolution Tem and Stem Imaging of Silicon Nanocrystals and Their Capping Ligands. *J. Phys. Chem. C* **2012**, *116*, 22463−22468.
(38) Mangolini, L.; Jurbergs, D.; Rogojina, E.; Kortshagen, U. Plasma Synthesis and Liquid-Phase Surface Passivation of Brightly Luminescent Si Nanocrystals. *J. Lumin.* **2006**, *121*, 327−334.
(39) Faulkner, D. O.; McDowell, J. J.; Price, A. J.; Perovic, D. D.; Kherani, N. P.; Ozin, G. A. Measurement of Absolute Photoluminescence Quantum Yields Using Integrating Spheres - Which Way to Go? *Laser Photonics Rev.* **2012**, *6*, 802−806.
(40) Lopinski, G. P.; Wayner, D. D. M. Molecular Monolayers on Silicon Surfaces. *Mater. Matters* **2008**, *32*, 38−41.
(41) Bullen, C.; Mulvaney, P. The Effects of Chemisorption on the Luminescence of Cdse Quantum Dots. *Langmuir* **2006**, *22*, 3007−3013.
(42) Hessel, C. M.; Rasch, M. R.; Hueso, J. L.; Goodfellow, B. W.; Akhavan, V. A.; Puvanakrishnan, P.; Tunnel, J. W.; Korgel, B. A. Alkyl Passivation and Amphiphilic Polymer Coating of Silicon Nanocrystals for Diagnostic Imaging. *Small* **2010**, *6*, 2026−2034.
(43) Lockwood, R.; Veinot, J. G. C.; Meldrum, A. Sensing Water and Alcohol Vapors with Freestanding Silicon Quantum Dots. *Sensor Lett.* **2013**, *11*, 1535−1540.
(44) Mei, B. C.; Oh, E.; Susumu, K.; Farrell, D.; Mountziaris, T. J.; Mattoussi, H. Effects of Ligand Coordination Number and Surface Curvature on the Stability of Gold Nanoparticles in Aqueous Solutions. *Langmuir* **2009**, *25*, 10604−10611.
(45) Wolkin, M. V.; Jorne, J.; Fauchet, P. M.; Allan, G.; Delerue, C. Electronic States and Luminescence in Porous Silicon Quantum Dots: The Role of Oxygen. *Phys. Rev. Lett.* **1999**, *82*, 197−200.
(46) Reboredo, F. A.; Galli, G. Theory of Alkyl-Terminated Silicon Quantum Dots. *J. Phys. Chem. B* **2005**, *109*, 1072−1078.
(47) Lockwood, R.; Hryciw, A.; Meldrum, A. Nonresonant Carrier Tunneling in Arrays of Silicon Nanocrystals. *Appl. Phys. Lett.* **2006**, *89*, 263112.
(48) Priolo, F.; Franzò, G.; Pacifici, D.; Vinciguerra, V.; Iacona, F.; Irrera, A. Role of the Energy Transfer in the Optical Properties of Undoped and Er-Doped Interacting Si Nanocrystals. *J. Appl. Phys.* **2001**, *89*, 264−272.
(49) Yang, J.; Liptak, R.; Rowe, D.; Wu, J.; Casey, J.; Witker, D.; Campbell, S. A.; Kortshagen, U. Uv and Air Stability of High-Efficiency Photoluminescent Silicon Nanocrystals. *Appl. Surf. Sci.* **2014**, *323*, 54−58.
(50) Froner, E.; Adamo, R.; Gaburro, Z.; Margesin, B.; Pavesi, L.; Rigo, A.; Scarpa, M. Luminescence of Porous Silicon Derived Nanocrystals Dispersed in Water: Dependence on Initial Porous Silicon Oxidation. *J. Nanopart. Res.* **2006**, *8*, 1071−1074.